ISBN: 978-3-95450-234-9 ISSN: 2673-5504 doi:10.18429/JACoW-SRF2023-TUIXA04

FIRST RESULTS FROM β-SRF— TESTING SRF SAMPLES AT HIGH PARALLEL FIELD

Edward Thoeng[1,2,*], Md Asaduzzaman[1,3], R. M. L. McFadden[1,3], J. O. Ticknor[1,4], P. Kolb[1], Gerald D. Morris[1], S. R. Dunsiger[1,6], D. Fujimoto[1], V. L. Karner[1], R. Li[1], M. Stachura[1], T. Junginger[1,3], R. F. Kiefl[1,2,5], W. Andrew MacFarlane[1,4,5], R. E. Laxdal[1,†]
[1]TRIUMF, Vancouver, Canada,
[2]Department of Physics & Astronomy, University of British Columbia, Vancouver, Canada
[3]Department of Physics & Astronomy, University of Victoria, Victoria, Canada
[4]Department of Chemistry, University of British Columbia, Vancouver, Canada
[5]Stewart Blusson Quantum Matter Institute, University of British Columbia, Vancouver, Canada
[6]Department of Physics, Simon Fraser University, Burnaby, Canada

Abstract

The new β-SRF facility at TRIUMF has recently been commissioned. A new 1 m extension has been added to an existing β-NMR beamline with a large Helmholtz coil to produce fields up to 200 mT parallel to sample surfaces. The β-NMR technique allows depth dependent characterization of the local magnetic field in the first 100 nm of the sample surface making the probe ideal for studying Meissner screening in heat treated Niobium or layered SRF materials. First measurements of Meissner screening at fields up to 200 mT have been analyzed. The results show clear differences in the Meissner screening of baseline treatments compared to mid-T baked (O-doped) Niobium.

INTRODUCTION

The SRF community has been successful at improving the high gradient and high quality factor (Q_0) performance of Niobium through empirically developed heat treatments in vacuum or with small concentrations of doping agents. The most successful recipes have been repeatable at multiple labs and also in industry. Future projects like the ILC require performance at high gradient to reduce costs. The development of robust recipes and processes is a critical goal of the present development. Researchers are also pursuing thin films and layered structures [1, 2] in order to either reduce the cost of Nb or increase the performance or operating temperature.

Niobium is a marginal Type-II superconductor. Raising the applied field past a critical value, B_{c1} leads to a mixed state in which an increasing amount of magnetic flux penetrates the material in quantized flux vortices. At a second critical field strength, B_{c2} superconductivity is destroyed. However, above B_{c1} a metastable state persists up to the superheating field, B_{sh} allowed by a surface energy barrier that inhibits vortex nucleation. As RF fields increase in amplitude, magnetic vortices with normal cores can nucleate in the near surface and RF losses, hence surface heating, occurs. For high gradient performance we need a material that can withstand vortex penetration up to a high peak magnetic field.

The intrinsic performance of SRF cavities is determined by the first 100 nm of the inner cavity surface, where RF currents flow with a length scale characterized by the London Penetration Depth. Cavity treatments impact the near-surface nanostructure in the first hundreds (or less) nanometers of the Niobium surface to improve Q_0 or gradient or both. The strategy moving forward will be to engineer a surface layer on bulk Nb to reproducibly optimize the performance beyond pure Nb. Thin film research and theory are continuing in parallel with work on NbN, Nb_3Sn, MgB_2 and Superconductor-Insulator-Superconductor (SIS) [1, 2] layers.

Investigations of new treatments and new materials would benefit from a diagnostic that provides details of the magnetic screening within the near surface. Ideally the probe should be able to diagnose the detailed magnetic screening near the critical fields which for Niobium is in the range of 200 mT. DC magnetic fields applied both perpendicular and parallel to the sample surface have been used as analogues of cavity operating conditions to characterize SRF materials with respect to the field of first flux penetration [3].

Perpendicular fields result in highly non-uniform surface fields when the sample is in the Meissner state, with flux accentuated at sample edges. Parallel fields on flat samples or ellipsoid samples provide near uniform surface fields up to the field of first flux penetration. Measurements typically record the maximum local surface field (based on the applied field and the sample geometry) that can be reached before flux is detected in the bulk. Such measurements do not provide local details of the role of the surface layer(s) in the field of first flux entry. Given the interest in layered structures and their precise role in enhancing the field of first flux entry, a diagnostic that provides the depth-resolved information of field attenuation through the London layer would provide new insight.

Facilities like β-NMR [4–6] (TRIUMF) and LE-muSR [7] (PSI) that use $^8Li^+$ ions or low energy muons respectively have been limited to <30 mT parallel field on the sample as the transverse fringe field from the applied

* ethoeng@triumf.ca
† lax@triumf.ca

ISBN: 978-3-95450-234-9 ISSN: 2673-5504 doi:10.18429/JACoW-SRF2023-TUIXA04

field deflects the low energy charged particle probe as the charged particle approaches the sample. Of the two techniques β-NMR with its heavier probe opens the door for exploitation of higher parallel fields.

We have now extended an existing beamline at TRIUMF called β-SRF [8] within the β-detected nuclear magnetic resonance facility at TRIUMF [4–6] (β-NMR) facility that provides up to 200 mT parallel to the surface of the sample. This paper will give an overview of the new facility and the results from a first experiment on two SRF samples.

β-NMR TECHNIQUE

β-NMR is a type of nuclear magnetic resonance (NMR) technique which utilizes implanted spin-polarized radioactive nuclei as probes [4–6]. In β-NMR the local magnetic field is monitored using the anisotropic emission of the β-particles (typically MeV energy), that are highly correlated with the direction of the nuclear spin at the time of the decay. The energetic βs are detected in two opposing detector telescopes (with pairs of scintillators in coincidence), oriented at 0 and π radians relative to the direction of the initial spin polarization. The time evolution of the (longitudinal) spin-polarization can be measured as the probe spin interacts with the local magnetic field inside the sample. A unique feature of the method is that the implantation energy of radioactive nucleii can be varied (e.g., from ~0.5 keV to ~30 keV) to study the surface of materials in a depth-resolved manner with nm length scale.

Several techniques have been developed to characterize materials with β-NMR . The spin-lattice relaxation (SLR) technique [9] is adopted for the results reported here. In the SLR technique, the applied field is parallel to the initial spin-polarization direction. Spin-polarization of the probe is lost through an energy exchange with its surrounding environment. That is, spontaneous, stochastic fluctuations in the local field that are transverse to the probe spin direction serve to "reorient" it back to thermal equilibrium while the applied field acts to slow the relaxation.

The SLR rate, commonly denoted as $1/T_1$, characterizes the depolarization time-constant of the ^{8}Li nuclear spins after they are stopped inside the sample. The value of $1/T_1$ is extracted by fitting the measured time-dependent asymmetry in the β-decay with a phenomenological depolarization function. Figure 1 shows a typical asymmetry spectrum and corresponding fit measured on a Nb sample (cut, etched, and annealed at 1400 °C) at 5 K using a 4 keV ^{8}Li$^+$ beam. The data corresponds to beam on (grey) and beam off time responses.

At applied magnetic fields below ~1 T, the dominant relaxation mechanism in Nb is due to cross relaxation between the ^{8}Li and the host Nb nuclear spins [10], which gives a Lorentzian dependence of $1/T_1$ on the local magnetic field according to:

$$1/T_1 = \frac{a}{b + \langle B(E)\rangle^2}, \quad (1)$$

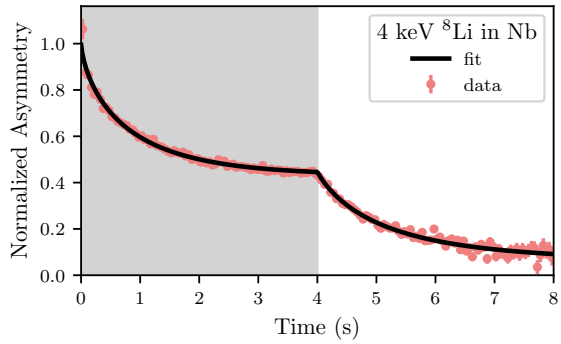

Figure 1: The time evolution of the normalized asymmetry for beam on (grey) and beam off.

where $\langle B(E)\rangle$ is the average measured local magnetic field, and a and b are material dependent fit parameters. The value of the fit parameters are determined by measuring $1/T_1$ values for known field levels.

β-NMR FACILITY AT TRIUMF

The β-NMR technique as implemented at TRIUMF requires a dedicated facility to produce high intensity radioactive ion beams (RIBs) with a high degree of spin polarization. In the case of TRIUMF, the high intensity RIBs, typically ^{8}Li , are produced at the Isotope Separator and Accelerator (ISAC) facility [11], which uses a 500 MeV cyclotron as a driver to bombard a solid radio-isotope production target with proton beams. The resulting short-lived nuclides are then ionized, extracted, and separated on-line to produce isotopically pure RIBs before being sent downstream for various experiments. Radioactive ^{8}Li$^+$ beams with an intensity of ~10^7 s^{-1} with polarization of 70% are routinely available. The spin polarization is done in-flight via collinear optical pumping with a circularly polarized resonant laser [12].

The TRIUMF β-NMR facility is shown in Fig. 2. At the end of each leg is a spectrometer assembly for sample measurements, containing the detectors, cold finger cryostat (for low temperature measurements), magnets, RF coil, HV deceleration (HV cage and deceleration electrodes), and charge-coupled device (CCD) imaging system. In addition, in order to achieve depth profiling, the sample ladder and cryostat are raised to the bias of the HV platform, which can be varied in order to decelerate the ion beam as it approaches the sample. The bias capability spans from 0 to 35 kV and typical beam energies are 20 to 30 keV.

There are two legs: the β-NMR leg and the β-NQR leg. On the β-NQR beamline, the (low parallel-field) spectrometer uses a normal conductor Helmholtz coil. The detectors are oriented to the left and right side of the sample, and up to four samples can be loaded simultaneously into the ultra-high vacuum (UHV) chamber via a sample ladder load-lock system.

ISBN: 978-3-95450-234-9 ISSN: 2673-5504 doi:10.18429/JACoW-SRF2023-TUIXA04

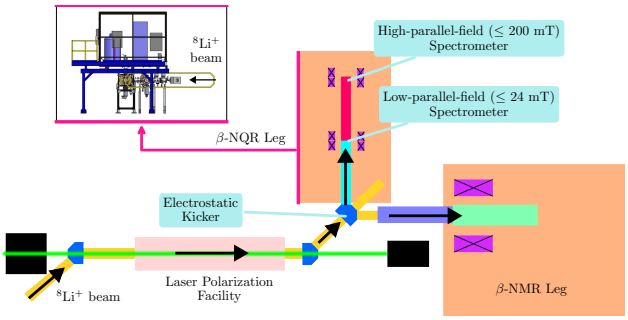

Figure 2: The β-NMR facility at TRIUMF.

β-SRF Facility

This paper reports the upgrade of the β-NQR leg with the addition of a 1 m long extension of the beamline to include a parallel field spectrometer capable of up to 200 mT for unique depth resolved studies of SRF and other materials [8]. A Helmholtz magnet generates the 200 mT at the Sample 2 location as shown in Fig. 3. Electrostatic quadrupoles are used to control the beam shape during transport and to focus the ions onto the sample and steering plates compensate for the vertical deflection due to the fringe field of the Helmholtz coil transverse to the beam direction.

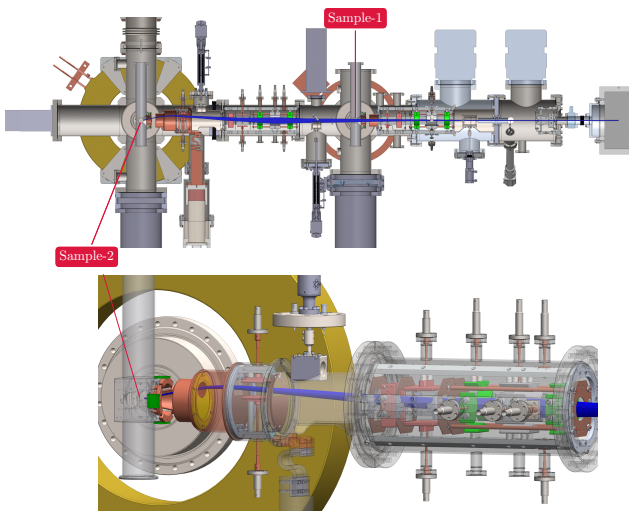

Figure 3: The β-NQR leg at the ISAC β-NMR facility. The ion beam is going from right to left. The sample 1 position is used for parallel fields up to 24 mT and the new β-SRFbeam line extension includes the ~1 m section downstream of sample 1 leading to the sample 2 position where fields up to 200 mT are possible. Superimposed on the beamline is the beam trajectory due to interaction of the beam with the fringe field of the Helmholtz coil.

An additional four-sector electrode (Figure 4) close to the sample (within ~50 mm) acts as a deceleration electrode, and allows independent horizontal and vertical steering which is used to compensate for the beam deflection and to re-center the beam on the sample. The fringe field diverts the beam by ~2.4 cm off-axis. Two vertical deflectors can be operated independently to achieve the desired beam path at lower fields (all the way down to zero-field).

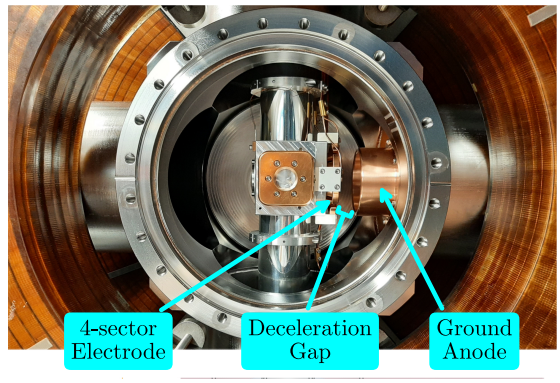

Figure 4: Side view of Helmholtz coil and sample chamber.

The ^{8}Li$^+$ beam was decelerated to a range of final energies range from 4 keV to 20 keV with Helmholtz magnet settings from 50 mT to 200 mT to establish optic settings. These tunes can be re-scaled for different beam energies, applied magnetic fields, and RIBs, as well as re-loaded (i.e., as a starting condition) to speedup future beam delivery. An example of a typical beamspot image is shown in Fig. 5, obtained at a parallel field of 200 mT. The image shows a 8 mm × 8 mm viewable (by CCD camera) section of the sapphire at the Sample 2 location. The average transverse beamspot dimensions (i.e., FWHM) at the sample is ~3 to 4 mm.

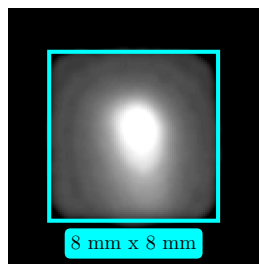

Figure 5: Beam image at the Sample 2 location for 200 mT.

FIRST EXPERIMENTS AT β-SRF

The experimental results presented here correspond to SLR measurements done on two samples. Each sample is tested at a range of applied parallel fields from 100 mT to 200 mT and for each applied field the depth profiles of the magnetic screening in the sample are measured by taking data at five different ^{8}Li$^+$ energies from 4 to 20 keV. Each sample is roughly a 10 mm × 10 mm flat slab of 2 mm thickness.

Sample A (Baseline sample) is a residual resistivity ratio (RRR) Nb slab that is annealed at 1400 °C for 4 h with a final flash BCP. Sample B (O-doped sample) is a Baseline sample further treated at 400 °C for 3 h in a typical mid-T bake recipe. The heat treatments are done in the TRIUMF

ISBN: 978-3-95450-234-9 ISSN: 2673-5504 doi:10.18429/JACoW-SRF2023-TUIXA04

RF induction oven. The dimension definitions are given in Fig. 6. The applied field is along the direction labelled 'c'.

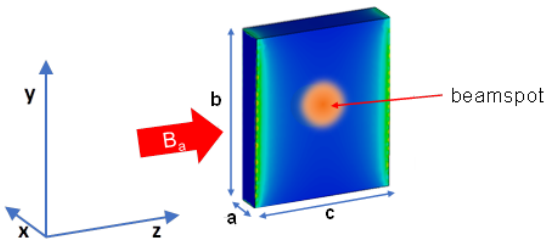

Figure 6: Reference geometry of the samples.

There are two key characteristics that need to be determined for each sample. In the Meissner state the sample will displace flux leading to an enhancement of the flux on the sample surface as compared to the applied field. The enhancement factor is determined in COMSOL [13] and confirmed in CST Studio [14] and the average value is determined by averaging over the beam spot of ~4 mm diameter. A second important parameter is the applied field where we would expect flux to break into the sample. Here we adopt the analysis of Brandt [15]. For Type-II superconducting slabs in the parallel geometry (Figure 7), flux will first break in at the corners and as the applied field increases the flux lines will extend deeper across the corner and eventually join at the centre where the now continuous flux line is driven inwards due to interaction with the surface currents to minimize the energy. The applied field where flux is driven into the sample we denote as B_{entry}. An empirical determination of the entry field for a flat slab is given by:

$$B_{\text{entry}} = B_{c1} \tanh \sqrt{0.36(c/a)}. \quad (2)$$

with an example of flux just before entry given in Fig. 7.

Figure 7: Flux lines just before entry into the sample [15].

Both the enhancement factor (ε-factor) and the entry field are geometry dependent. The two samples have similar but not identical geometries and result in different ε-factor and B_{entry} values. A summary of the sample dimensions and magnetic field characteristics are given in Table 1. The absolute B_{entry} is calculated assuming a B_{c1}=180 mT at 0 K and evaluating the critical field at the operational temperature of 4.5 K using:

$$B_{c1}(T) = B_{c1}(0)\left[1 - \left(\frac{T}{T_c}\right)^2\right], \quad (3)$$

where T_c is the critical temperature at zero applied field.

The average implantation depths are computed using the Stopping and Range of Ions in Matter (SRIM) package [16]. The ion depth increases with energy as does the broadening of the range as shown in Fig. 8. The implantation distribution of the ions for each energy is used to correlate the spatial field distribution to the field distribution measured as a function of energy.

Table 1: Sample Dimensions

Parameter	Baseline	O-Doped
a (mm)	1.8	1.7
b (mm)	8.1	12.5
c (mm)	9.8	12.6
ε	1.07	1.04
B_{entry}/B_{c1}	0.885	0.926
B_{entry} (mT) @ 4.5 K	121	127

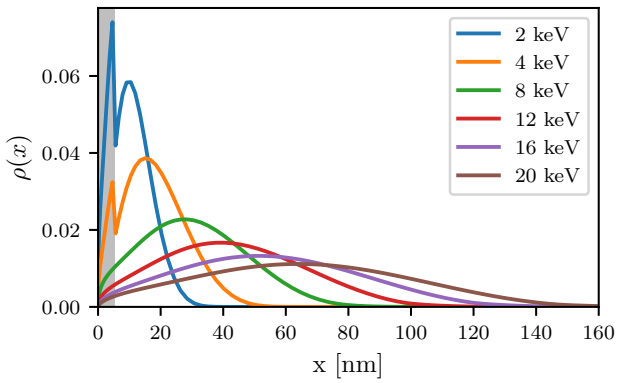

Figure 8: Implantation distribution of $^8Li^+$ ions in Nb with 5 nm of Nb_2O_5 native pentoxide (grey) overlayer.

Results

The samples are loaded into a target ladder so that samples can be exchanged without venting the cryostat. Each sample is tested at applied fields of 100, 110, 125, 150 and 200 mT. For each value the sample is first cooled to 4.5 K in zero-field and then the field is applied starting with the lowest field first. For each applied field the relaxation data is taken at implantation energies of 3.8, 7.9, 11.9, 15.9 and 19.9 keV. The relaxation rate, $1/T_1$, is computed in each case and plotted in Fig. 9 for the Baseline sample and in Fig. 10 for the O-doped sample.

There are several features of note. The depolarization rate for lower applied fields is higher than for higher average fields since it is the magnitude of the field sensed by the ^{8}Li that delays the relaxation. The rising slope of $1/T_1$ for lower applied fields as a function of implantation energy is a clear indication of Meissner screening. Note that at 200 mT the $1/T_1$ values are independent of depth indicating that the flux has fully broken into the sample.

The $1/T_1$ values are explicitly mapped to $\langle B(E)\rangle$ values by fits to the a and b Lorentzian parameters. The details of the data analysis will be presented in a paper now in preparation. This mapping results in the energy dependent screening profiles show in Figs. 11 and 12 for the Baseline and O-doped samples respectively. Note that for the Base-

ISBN: 978-3-95450-234-9 ISSN: 2673-5504 doi:10.18429/JACoW-SRF2023-TUIXA04

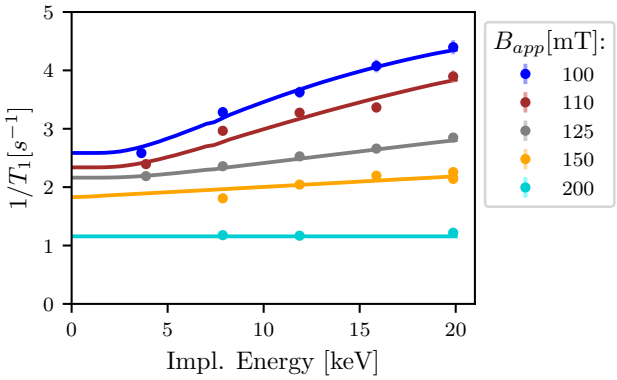

Figure 9: Experimental results for the Baseline sample. Shown are the relaxation rate as a function of implantation energy for various applied parallel fields.

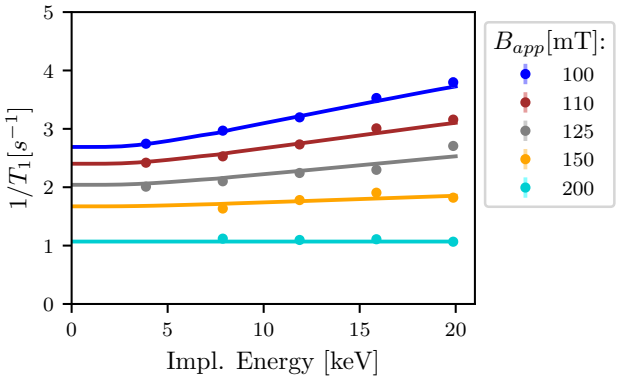

Figure 10: Experimental results for the O-doped sample. Shown are the relaxation rate as a function of implantation energy for various applied parallel fields.

line the applied fields of 100 mT and 110 mT have strong screening profiles indicative of the Meissner state while at 125 mT there is a marked slope change consistent with some flux breaking into the surface. This can be contrasted with the O-doped sample where the screening profile is longer than the Baseline sample but all of the 100, 110 and 125 mT applied fields look to have screening profiles consistent with the Meissner state.

Extracted data from the analysis of the two samples are given in Tables 2 and 3 for the Baseline sample and O-Doped sample respectively. Given are the applied field, the field enhancement factor, the ratio of the applied field to the anticipated entry field and the screening profile depth (SPD). Note that the London penetration depth at an applied field of 100 mT is 40 nm for the Baseline sample but almost three times longer in the O-doped sample consistent with a much dirtier near surface. Further, there is a distinct change in slope of the screening profile as the field increases indicating the transition from the Meissner state to the mixed state and that this slope transition is consistent with the expected entry field. Also note that in both samples the measured enhancement factor shifts towards unity when B_{applied} increases beyond B_{entry}.

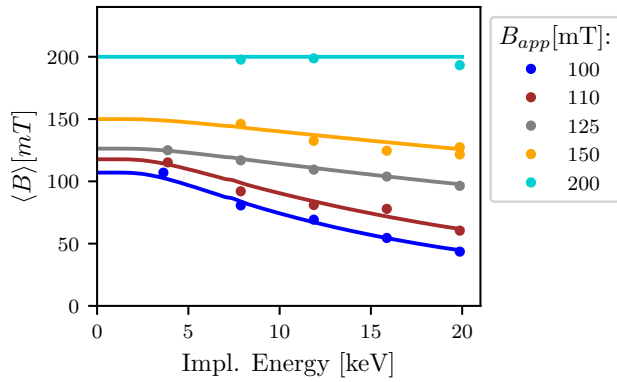

Figure 11: Baseline sample: Shown are the average B field as a function of implantation energy for various applied parallel fields.

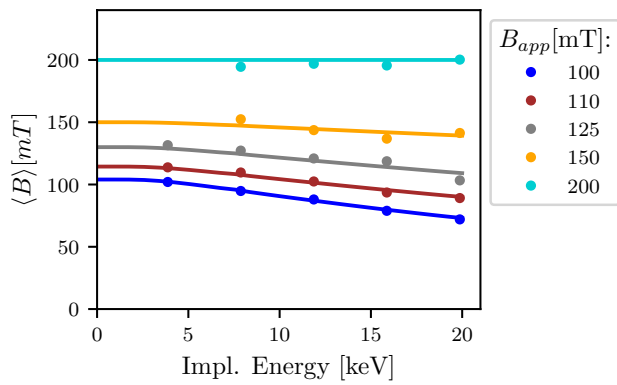

Figure 12: O-doped sample: Shown are the average B field as a function of implantation energy for various applied parallel fields.

The screening profiles plotted as a function of depth into the material are given in Figs. 13 and 14 for the Baseline and O-doped samples respectively. These plots clearly show the transition of the screening profile below and above B_{entry}.

SUMMARY

We have successfully completed a verification experiment at the new β-SRF facility at TRIUMF with parallel fields up to 200 mT for two samples, Baseline and O-doped. The measurements show that the screening profile is significantly longer in the O-doped sample compared to the Baseline sample, that the screening profile in the Meissner state near B_{c1} increases with applied field, and that there is a clear slope change in screening profile when the Meissner state transitions to the mixed state.

Table 2: Measured Parameters of the Baseline Sample

B_{applied}	$B_{\text{surf}}/B_{\text{applied}}$	$B_{\text{applied}}/B_{\text{entry}}$	SPD
100	1.07	0.83	40
110	1.07	0.91	59
125	1.01	1.03	167
150	1.00	1.24	250
200	1.00	1.65	N/A

ISBN: 978-3-95450-234-9 ISSN: 2673-5504 doi:10.18429/JACoW-SRF2023-TUIXA04

Table 3: Measured Parameters of the O-doped Sample

$B_{applied}$	$B_{surf}/B_{applied}$	$B_{applied}/B_{entry}$	SPD
100	1.04	0.79	117
110	1.04	0.87	178
125	1.04	0.99	248
150	1.00	1.18	600
200	1.00	1.58	N/A

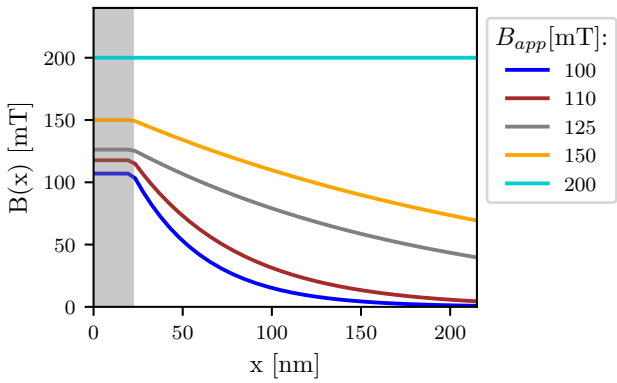

Figure 13: Baseline sample: Shown are the extracted B field as a function of implantation depth for various applied parallel fields. Shaded area (grey) indicates the dead layer.

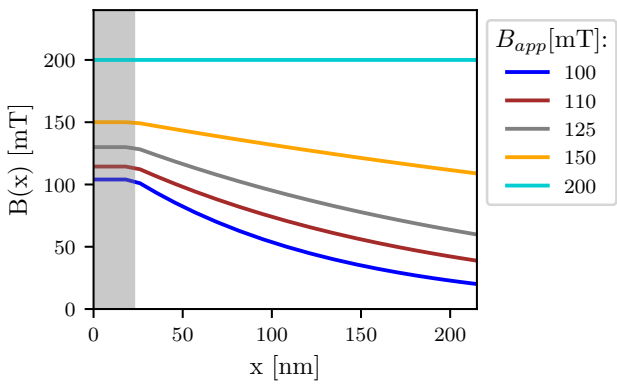

Figure 14: O-doped sample: Shown are the extracted B field as a function of implantation depth for various applied parallel fields. Shaded area (grey) indicates the dead layer.

CONCLUSION

β-SRF with high parallel field up to 200 mT near B_{c1} and variable implantation depth makes it ideal for characterizing new treatments, new materials and layered structures. β-SRF is the only facility in the world where such depth dependent measurements can be done with magnetic fields that replicate RF field amplitudes near the fundamental limits of Niobium.

ACKNOWLEDGEMENTS

This project is funded through Research Tools and Infrastructure grant from NSERC (Natural Science and Engineering Research Council).

REFERENCES

[1] A. Gurevich, "A. Maximum screening fields of superconducting multilayer structures", *AIP Adv.*, vol. 5, p. 017112, 2015. doi:10.1063/1.4905711

[2] T. Kubo, "Multilayer coating for higher accelerating fields in superconducting radio-frequency cavities: a review of theoretical aspects", *Supercond. Sci. Technol.*, vol. 30, p. 023001, 2016. doi:10.1088/1361-6668/30/2/023001

[3] T. Junginger *et al.,* "Field of first magnetic flux entry and pinning strength of superconductors for rf application measured with muon spin rotation", *Phys. Rev. Accel. Beams*, vol. 21, p. 032002, 2018. doi:10.1103/PhysRevAccelBeams.21.032002

[4] W. A. MacFarlane, "Implanted-ion βNMR: A new probe for nanoscience", *Solid State Nucl. Magn. Reson.* vol. 1, pp. 68-69, 2015. doi;10.1016/j.ssnmr.2015.02.004

[5] W. A. MacFarlane, "Status and progress of ion-implanted βNMR at TRIUMF", *Z. Phys. Chem.*, vol. 236, pp. 757-798, 2022. doi:10.1515/zpch-2021-3154

[6] G. Morris, "β-NMR", in *ISAC And ARIEL: The TRIUMF Radioactive Beam Facilities And The Scientific Program*, Springer, pp. 173-182, 2014. doi:10.1007/978-94-007-7963-1_19

[7] A. F. A. Simões *et al.*, "Muon implantation experiments in films: Obtaining depth-resolved information", *Rev. Sci. Instrum.*, vol. 91, p. 023906, 2020. doi:10.1063/1.5126529.

[8] E. Thoeng *et al.*, "A new high parallel-field spectrometer at TRIUMF's β-NMR facility", *Rev. Sci. Instrum.*, vol. 94, p. 023305, 2023. doi:10.1063/5.0137368

[9] C. P. Slichter, "Spin-Lattice Relaxation and Motional Narrowing of Resonance Lines", in *Principles of Magnetic Resonance*, Springer Series in Solid-State Sciences, vol 1. Springer, Berlin, Heidelberg, 1990. doi:10.1007/978-3-662-09441-9_5

[10] T. Parolin *et al.*, "MacFarlane, W. Nuclear magnetic resonance study of Li implanted in a thin film of niobium", *Phys. Rev. B*, vol. 80, p. 174109, 2009. doi:10.1103/PhysRevB.80.174109

[11] J. Dilling and R. Krücken, "The experimental facilities at ISAC", in *ISAC and ARIEL: The TRIUMF Radioactive Beam Facilities and the Scientific Program*, pp. 111-114, 2014. doi:10.1007/978-94-007-7963-1_10

[12] C. Levy, M. Pearson, R. Kiefl, E. Manè, G. orris, and A. Voss, "Laser polarization facility", in *ISAC And ARIEL: The TRIUMF Radioactive Beam Facilities And The Scientific Program.* pp. 165-172, 2014. doi:10.1007/978-94-007-7963-1_18.

[13] COMSOL Multiphysics®, http://www.comsol.com

[14] CST Studio Suite, https://www.3ds.com/products-services/simulia/products/cst-studio-suite/.

[15] E. Brandt, "Superconductors in realistic geometries: geometric edge barrier versus pinning", *Physica C: Superconductivity*, vol. 332, pp. 99-107, 2000. doi:10.1016/S0921-4534(99)00651-6.

[16] J. F. Ziegler *et al.*, "SRIM - The stopping and range of ions in matter", *Nucl. Instrum. Methods Phys. Res., Sect. B.* vol. 268, p. 1818, 2010. doi:10.1016/j.nimb.2010.02.091.